17. W. J. Borucki, M. A. Williams, *J. Geophys. Res.* **91**, 9893 (1986).
18. S. J. Weidenschilling, J. S. Lewis, *Icarus* **20**, 465 (1973).
19. C. P. Porco *et al.*, *Science* **299**, 1541 (2003).
20. A. P. Ingersoll *et al.*, *J. Geophys. Res.* **86**, 8733 (1981).
21. S. S. Limaye, *Icarus* **65**, 335 (1986).
22. M. Allison, *Icarus* **83**, 282 (1990).
23. K. H. Baines, R. W. Carlson, L. W. Kamp, *Icarus* **159**, 74 (2002).
24. P. J. Gierasch *et al.*, *Nature* **403**, 628 (2000).
25. A. P. Ingersoll, C. C. Porco, *Icarus* **35**, 27 (1978).
26. I. A. Pirraglia, *Icarus* **59**, 169 (1984).
27. D. C. Reuter *et al.*, *Space Sci. Rev.*, in press (available at http://arxiv.org/abs/0709.4281v1).
28. Galileo NIMS global maps were acquired on 5 September 1996 from a distance of $1.98 \times 10^6$ km, a phase angle of 64.3°, a subsolar latitude near 2°S, and a subspacecraft latitude near 0°. A Cassini Imaging Science Subsystem global image was acquired on 29 December 2000 from a distance of approximately $1.0 \times 10^6$ km, a phase angle near 90°, a subsolar latitude near 2.9°N, and a

subspacecraft latitude near 3.5°N. A New Horizons LEISA global map was acquired on 28 February 2007 in three north/south scans over a 47-min period beginning at 01:40 universal time (UT) on 28 February from an altitude of $2.32 \times 10^6$ km, a phase angle of 76°, a subsolar latitude near 2.9°S, and a subspacecraft latitude of 8.4°S. The three-color image (middle right of Fig. 2), is composed of a 1.59-μm continuum wavelength image (red), a 1.90-μm wavelength image of moderate atmospheric gas absorption (green), and a 1.85-μm wavelength image of relatively strong absorption gas (blue). Blue accentuates high-altitude clouds and hazes above the 300 mbar level, green depicts clouds most prominently near and above the 600-mbar level, and red shows clouds down to several bars. The 4.8-μm pseudo-color images were acquired at NASA's Infrared Telescope Facility (IRTF) at 10:08 UT on 30 December 2000 by the National Science Foundation camera (NSFCam) camera and on 18 March 2007 at 14:53 UT by the NSFCam2 camera. The 17.9-μm images were acquired by the Jet Propulsion Laboratory's MIRLIN (Mid-Infrared Large-well Imager) camera (32) at 5:50 UT on 29 December 2000 and by the MIRSI (Mid-Infrared

Spectrometer and Imager) camera/spectrometer (33) at 16:12 UT on 18 March 2007.
29. A. R. Vasavada *et al.*, *Icarus* **135**, 265 (1998).
30. D. C. Reuter *et al.*, *Science* **318**, 223 (2007).
31. W. J. Borucki, C. P. McKay, D. Jebens, H. S. Lakkaraju, C. T. Vanajakshi, *Icarus* **123**, 336 (1996).
32. M. E. Ressler *et al.*, *Exp. Astron.* **3**, 277 (1994).
33. L. Deutsch, *et al.*, *SPIE* **4841**, 106 (2002).
34. We thank the New Horizons mission and science teams. New Horizons is funded by NASA. G.S.O., P.Y.F., and B.M.F. were visiting astronomers at the IRTF, which is operated by the University of Hawaii under Cooperative Agreement no. NCC-538 with NASA, Science Mission Directorate, Planetary Astronomy Program. Thanks to E. Tollestrup and M. Connelley for IRTF instrument orientation and J. Kemerer· and J. Yang for assistance in reducing the observations. Much of the work described in this paper was carried out at the Jet Propulsion Laboratory, Pasadena, CA, under contract with NASA.

# REPORT

# Jupiter's Nightside Airglow and Aurora

G. Randall Gladstone,[1]* S. Alan Stern,[2] David C. Slater,[1] Maarten Versteeg,[1] Michael W. Davis,[1] Kurt D. Retherford,[1] Leslie A. Young,[3] Andrew J. Steffl,[3] Henry Throop,[3] Joel Wm. Parker,[3] Harold A. Weaver,[4] Andrew F. Cheng,[2] Glenn S. Orton,[5] John T. Clarke,[6] Jonathan D. Nichols[6]

Observations of Jupiter's nightside airglow (nightglow) and aurora obtained during the flyby of the New Horizons spacecraft show an unexpected lack of ultraviolet nightglow emissions, in contrast to the case during the Voyager flybys in 1979. The flux and average energy of precipitating electrons generally decrease with increasing local time across the nightside, consistent with a possible source region along the dusk flank of Jupiter's magnetosphere. Visible emissions associated with the interaction of Jupiter and its satellite Io extend to a surprisingly high altitude, indicating localized low-energy electron precipitation. These results indicate that the interaction between Jupiter's upper atmosphere and near-space environment is variable and poorly understood; extensive observations of the day side are no guide to what goes on at night.

Jovian dayside airglow and aurora have been extensively observed from Earth orbit since their initial detection during the Voyager flybys in 1979 (1–8). On 3 March 2007 between 06:28 and 09:58 universal time (UT) (about 3 days after closest approach on 28 February at 05:43 UT) during the flyby of Jupiter, the New Horizons spacecraft made several high phase-angle observations of nightside airglow (nightglow) and auroral emissions. Because the night side has not been well observed, long-standing questions remain, including the nature of Jupiter's 121.6-nm (Lyα) nightglow (for example, is it similar to the tropical arcs of Earth?), how the nightside auroras are different from those on the

day side, and what the smallest structures in satellite footprint auroras are and what governs their size.

Jupiter's nightside hydrogen Lyα airglow was seen by Voyager 2 in 1979. Data from its ultraviolet (UV) spectrometer showed substantial nonauroral emissions well past the terminator, which were interpreted to result from low-latitude particle precipitation (1, 2). Low-latitude particle precipitation was also suggested as a way to maintain Jupiter's large exospheric temperature (9) and to account for low-latitude x-ray emission (10). In contrast, several nightside east-west scans by the Alice UV spectrograph on New Horizons (11, 12) indicate that the Lyα nightglow is faint, and there was no evidence of emission from high solar zenith angle regions on the night side that are far from the auroral regions (Fig. 1). Instead, the emissions are well fit by scattered solar Lyα radiation from the bright limb (13). This finding implies that no substantial low-latitude particle precipitation is currently occurring and suggests that either the Voyager results were spurious or Jupiter has changed between the two epochs (the Voyager flybys

were during solar maximum, whereas the New Horizons flyby occurred during solar minimum).

Observations of Jupiter's night side also provide a way to search for the presence of tropical arcs, which at Earth are bands of emission on either side of the magnetic equator resulting from the recombination of ions and are useful tracers of ionospheric dynamics (14, 15). The Lyα dayglow of Jupiter is known from Voyager Ultraviolet Spectrometer results to have a bulge of brightness that follows the magnetic dip equator (16). A possible explanation for the Lyα bulge is extra scattering of solar Lyα radiation from a hot hydrogen population resulting from $H_3^+$ recombination on either side of the magnetic equator; that is, the bulge might resolve into tropical arcs if seen at higher spatial resolution (17). Although no large-scale Lyα nightglow was seen by New Horizons, there are indications of excess brightening near the terminator, especially in regions where tropical arcs might be expected (such as near the end points of the low-latitude magnetic field line traces in Fig. 1).

Most of Jupiter's UV aurora results from collisions of energetic magnetospheric electrons with atmospheric hydrogen, leading to emissions at wavelengths from 80 to 165 nm. However, the more energetic electrons penetrate deeper into the atmosphere, where the resulting shorter-wavelength UV auroral emissions can be partially absorbed by atmospheric methane. The color ratio is defined as the ratio of the integrated auroral brightness from 155.7 to 161.9 nm over that from 123.0 to 130.0 nm (18, 19) and is used as a proxy for the mean energy of auroral electrons. A larger color ratio results from preferential absorption of shorter-wavelength UV photons by hydrocarbons (primarily $CH_4$) overlying a deeper layer of auroral emissions. Data from the Space Telescope Imaging Spectrograph (STIS) on the Hubble Space Telescope (HST) (20) and the Ultraviolet Imaging Spectrograph on Cassini (21) show that typical color ratios were 1.5 to 6.0 and that the largest ratios (and presumably

[1]Southwest Research Institute, San Antonio, TX 78238, USA. [2]NASA Headquarters, Washington, DC 20546, USA. [3]Southwest Research Institute, Boulder, CO 80302, USA. [4]The Johns Hopkins University Applied Physics Laboratory, Laurel, MD 20723, USA. [5]Jet Propulsion Laboratory, Pasadena, CA 91109, USA. [6]Boston University, Boston, MA 02215, USA.

*To whom correspondence should be addressed. E-mail: rgladstone@swri.edu

the most energetic precipitating electrons) occurred over the morning or dawn side of the northern main auroral oval (as seen from Earth). In contrast, both the total UV brightness and the color ratios inferred from the Alice nightside scans (Fig. 2) are largest on the dusk side of the northern main au-roral oval (regardless of the orientation of the oval in system III longitude). The implication is that variations in the mean energy of the precipitating electrons do not rotate with the planet in system III (along with the pattern of the main oval), but instead are controlled by solar local time, with the post-dawn daytime (20, 21) and post-dusk night-time (Fig. 2) regions experiencing the hardest au-roral electrons. The electrons responsible for the post-dusk nighttime emissions seen by Alice are most likely connected to the dusk flank of the mag-netosphere, which is likewise approximately fixed in



**Fig. 1.** East-west disk scans of the atomic hydrogen Lyα nightglow brightness across Jupiter obtained by the New Horizons Alice UV spectrograph on 3 March 2007. The long axis of the Alice 0.1° × 4° slit was aligned north-south, and the scan proceeded from the night side (right) toward the daylit crescent (left). The tracks (dashed white lines) and model-simulated Lyα brightnesses (solid white lines) for specific 0.1° × 0.3° pixels (row numbers are given at the right; the Alice boresight is located in the row-16 pixel) along the Alice slit and examples of their footprints (white boxes) are indicated on a simulated Lyα image (as would be seen from the spacecraft range, latitude, and system III longitude of 78.9 jovian radii, 2.1°N, and 133.0°, respectively). Alice-measured Lyα brightnesses (starting at 06:28 UT at the spacecraft, at a phase angle of 153.6°) are shown (vertical white lines, representing measured values ±1σ during 10-s intervals); both model and measured brightnesses use their associated tracks (dashed white lines) as abscissas. The color bar at the bottom provides model image brightnesses in kilorayleighs (kR). The ovals of the main UV aurora and Io's orbit footprint are shown in red and orange, respectively. Also shown are VIP4 model (31) surface magnetic field strengths in Gauss (green contours) and model traces of low-latitude magnetic field lines having peak altitudes of 1500 km above the 1-bar pressure level along the magnetic dip equator, plotted every 5° of longitude (green vertical lines). The white dotted lines are planetographic latitude and longitude at 30° intervals.
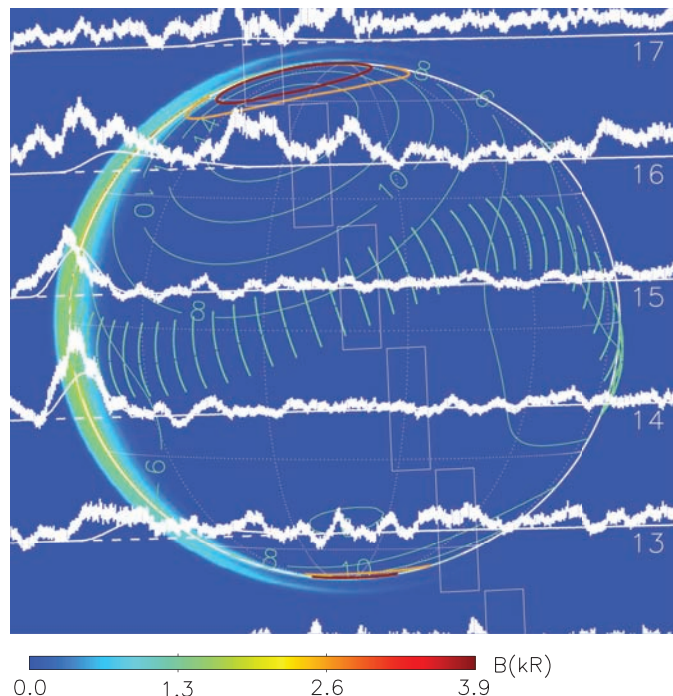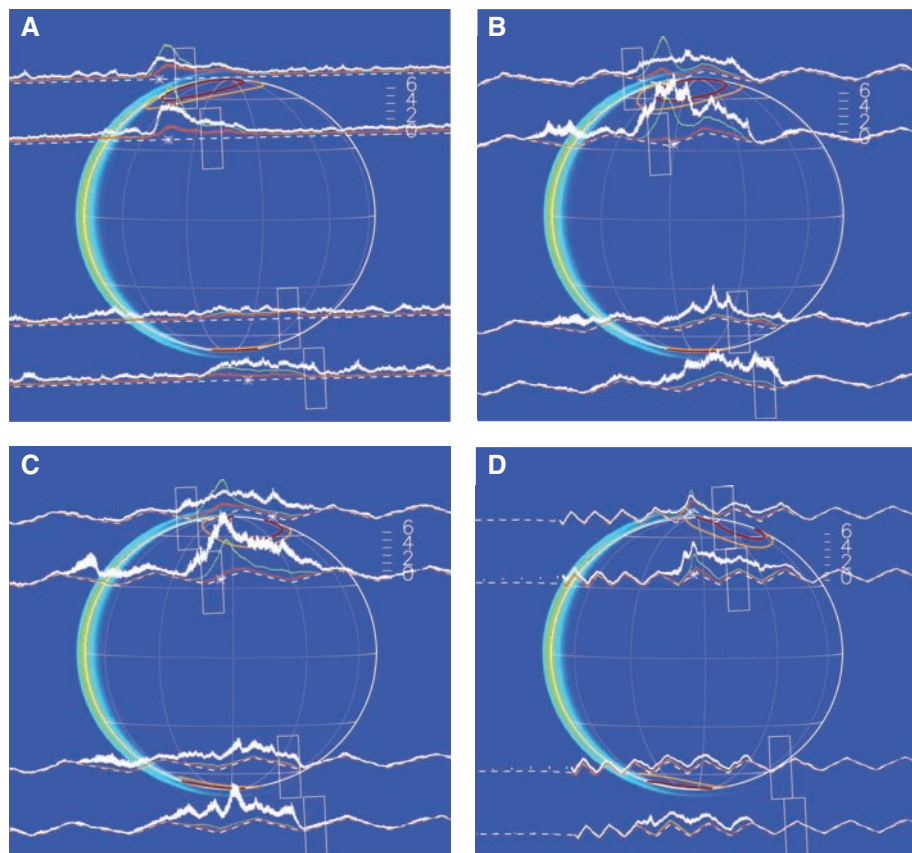
**Fig. 2.** Four east-west nightside auroral scans obtained by the New Horizons Alice UV spectrograph on 3 March 2007, starting at 06:28 UT (**A**), 07:28 UT (**B**), 08:38 UT (**C**), and 09:28 UT (**D**) (at the spacecraft). Auroral brightnesses in two wavelength bands are shown superposed on simulated Lyα images (Fig. 1). The ±1σ measured brightnesses are shown for emissions with wavelengths in the range from 155.7 to 161.9 nm (green lines) and in the range from 123.0 to 130.0 nm (rust-colored lines). The ratio of these two brightnesses gives the "color ratio" (18, 19): a common proxy for auroral electron energy. The ±1σ derived color ratios along each scan are shown (solid white lines), and a numbered grid on the second scan from the top provides the scale (measured from the scan tracks shown by the white dashed lines; non-uniform tracks result from spacecraft attitude corrections). A white asterisk marks the location of maximum color ratio along each track. Other features are as described for Fig. 1. The peak color ratios observed in Alice row 16 (the second row from the top in each panel) are 4.5 (A), 8.5 (B), 8.1 (C), and 4.1 (D).
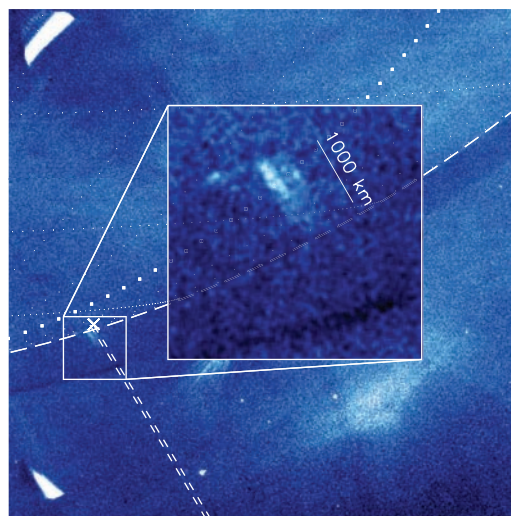
solar local time (22). This observation is surprising; however, other features of the main oval are also modified by local time, such as the bright dawn storms, which are always seen near the dawn limb (23). Likewise, the width of the main oval seems to always be narrower in the morning than the evening, irrespective of longitude (24). The Alice data imply that the mean energy of precipitating electrons varies with local time across the night side of Jupiter.

The Io Flux Tube (IFT) comprises Jovian magnetic field lines that are transiently interacting with the atmosphere of the satellite Io. At the footprint of the IFT in Jupiter's upper atmosphere, a spot and associated downstream tail of emission are seen in UV (and near-infrared) wavelengths (25, 26). The limb profile of the southern IFT footprint was observed (Fig. 3) by the New Horizons Long Range Reconnaissance Imager (LORRI) high-resolution visible imager during a series of 16 5-s exposures meant to establish peak auroral emission altitudes where the ovals cross the limb. Although the signal-to-noise ratio of the images is low, at ~28 km per pixel, this resolution is comparable to images obtained by Galileo (24). The visible emissions, which are probably mostly due to the Balmer series of atomic H lines and low-level $H_2$ bands, extend to high altitudes (>1000 km) above the limb. The integrated signal in the IFT profile measured at the spacecraft is $5 \times 10^{-10}$ to $7 \times 10^{-10}$ erg/cm$^2$/s; the emitted power is ~0.1 to 0.15 GW. The high altitudes indicate that either the electron precipitation was relatively soft or the atmosphere was highly disturbed, or both. Indeed, substantial soft electron precipitation would be expected to greatly disturb the high-altitude atmosphere (because of its low heat capacity), if the region affected weren't so

localized (27). In contrast, previous HST STIS measurements of the IFT footprint color ratio are in the range from 1.7 to 2.3, showing the effects of absorption by methane and indicating that most of the precipitating electrons in the IFT penetrate to much lower altitudes, between ~200 and 300 km (28). The width of the IFT flux tube emission seen in Fig. 3 has an overall value of about 400 km, which maps to about three Io diameters at the satellite (that is, localized near Io). In addition, there appears to be a parallel substructure to the emission, consistent with the expected current loop connecting to the sub-Jupiter and anti-Jupiter points on Io (29, 30). However, it is also possible that the substructure results from the projection of a secondary spot located farther downstream (at lower longitude). A spot of emission noticeable on the limb to the left of the main emissions could be a precursor spot (in which case it is produced by electrons that are substantially more energetic than those responsible for the main IFT emissions), or it could be the highest-altitude emissions of a spot farther downstream just peaking above the limb, although that seems unlikely. UV images obtained by the Advanced Camera for Surveys (ACS) on the HST during the time of the New Horizons observations also show the IFT emissions at high altitude. The HST ACS data (100-s exposures, 125 km per pixel) do not exhibit multiple spots, although the observing geometry is poor (supporting online material). It may be that the IFT auroral electrons are generally less energetic when Io is on the night side of Jupiter. Further analysis of the IFT footprint morphology (for example, using the extensive data set of HST ACS observations) may be useful for determining whether there is a local time dependence in the vertical extent of the emissions.

**References and Notes**
1. A. L. Broadfoot et al., J. Geophys. Res. **86**, 8259 (1981).
2. J. C. McConnell, B. R. Sandel, A. L. Broadfoot, Icarus **43**, 128 (1980).
3. A. Bhardwaj, G. R. Gladstone, Rev. Geophys. **38**, 295 (2000).
4. T. G. Slanger, B. C. Wolven, in Atmospheres in the Solar System: Comparative Aeronomy, M. Mendillo, A. Nagy, J. H. Waite Jr., Eds. (American Geophysical Union, Washington, DC, 2002), pp. 77–93.
5. D. Grodent et al., J. Geophys. Res. **108**, 1366 (2003).
6. D. Grodent et al., J. Geophys. Res. **108**, 1389 (2003).
7. J. T. Clarke et al., in Jupiter: The Planet, Satellites and Magnetosphere, F. Bagenal, T. E. Dowling, W. B. McKinnon, Eds. (Cambridge Univ. Press, Cambridge, 2004), pp. 639-670.
8. R. V. Yelle, S. Miller, in Jupiter: The Planet, Satellites and Magnetosphere, F. Bagenal, T. E. Dowling, W. B. McKinnon, Eds. (Cambridge Univ. Press, Cambridge, 2004), pp. 185–218.
9. D. M. Hunten, A. J. Dessler, Planet. Space Sci. **25**, 817 (1977).
10. J. H. Waite Jr. et al., Science **276**, 104 (1997).
11. S. A. Stern et al., Proc. SPIE **5906**, 358 (2005).
12. D. C. Slater et al., Proc. SPIE **5906**, 368 (2005).
13. The data reduction uses an effective area for Lyα of 0.007 cm$^2$, as determined from comparison of International Ultraviolet Explorer and Alice cruise-phase observations of the bright UV stars γ Gru (HD 207971) and ρ Leo (HD 91316). The model used is described in (17) and calculates resonantly scattered sunlight for a Jupiter atmosphere with 0.1% hot hydrogen, which provided the best fit to Galileo data. The solar Lyα flux (~3.8 × 10$^{11}$ photons/cm$^2$/s at Earth), corrected for the distance to Jupiter and the angle between Earth and Jupiter as seen from the Sun, is from Solar Radiation and Climate Experiment data at http://lasp.colorado.edu/sorce/data/data_product_summary.htm.
14. E. V. Appleton, Nature **157**, 691 (1946).
15. A. B. Christensen, et al., J. Geophys. Res. **108**, 1451 (2003).
16. A. J. Dessler, B. R. Sandel, S. K. Atreya, Planet. Space Sci. **29**, 215 (1981).
17. G. R. Gladstone et al., Planet. Space Sci. **52**, 415 (2004).
18. Y. L. Yung et al., Astrophys. J. **254**, L65 (1982).
19. T. A. Livengood, H. W. Moos, G. E. Ballester, R. M. Prangé, Icarus **97**, 26 (1992).
20. J. Gustin, D. Grodent, J. C. Gérard, J. T. Clarke, Icarus **157**, 91 (2002).
21. J. M. Ajello et al., Icarus **178**, 327 (2005).
22. K. K. Khurana, et al., in Jupiter: The Planet, Satellites and Magnetosphere, F. Bagenal, T. E. Dowling, W. B. McKinnon, Eds. (Cambridge Univ. Press, Cambridge, 2004), pp. 593–616.
23. J. T. Clarke et al., J. Geophys. Res. **103**, 20217 (1998).
24. A. R. Vasavada et al., J. Geophys. Res. **104**, 27133 (1999).
25. J. E. P. Connerney, R. L. Baron, T. Satoh, T. Owen, Science **262**, 1035 (1993).
26. R. Prangé et al., Nature **379**, 323 (1996).
27. Even if there were no high-altitude winds to disperse the heat from the IFT footprint aurora, because of Io's orbital motion, the IFT footprint moves westward through the local atmosphere at ~5 km/s and so traverses its ~400-km width in about 80 s.
28. J.-C. Gérard et al., J. Geophys. Res. **107**, 1394 (2002).
29. J. Saur et al., J. Geophys. Res. **104**, 25105 (1999).
30. D. H. Pontius, J. Geophys. Res. **107**, 1165 (2002).
31. J. E. P. Connerney, M. H. Acuna, N. F. Ness, T. Satoh, J. Geophys. Res. **103**, 11929 (1998).
32. We thank the New Horizons mission team and the New Horizons science team. New Horizons is funded by NASA, whose financial support we gratefully acknowledge. G.R.G. thanks H. Waite, W. Lewis, D. Pontius, D. Grodent, and J.-C. Gérard for comments and D. Grodent for providing locations of the main auroral and Io ovals.

**Fig. 3.** IFT footprint limb profile as imaged by the New Horizons LORRI panchromatic camera in a 5-s exposure of Jupiter's nightside south auroral region on 3 March 2007, centered at 09:19:07.9 UT. Scattered sunlight from the nearby bright limb (the solar elongation was ~26°) results in many artifacts at this stretch of the image, many of which have been removed (and several are covered by the inset image). The IFT profile (highlighted in the inset) shows up near its expected location in four separate images, of which this is the sharpest. The predicted location of the IFT footprint is just beyond the limb, as indicated by the white cross (at a planetographic latitude of 74.1°S and a system III longitude of 135.9°; the spacecraft was at a range of 5,810,940 km, a latitude of 2.2°N, and a system III longitude of 229.6°). Projected IFT magnetic field lines are shown (dashed lines); the right line connects to a location separated from the center of Io by 3642 km; that is, one Io diameter, toward Jupiter; the left line to a location the same separation from the center of Io away from Jupiter. A 10° graticule of Jupiter is overplotted with planetographic latitudes and longitudes at 1° spacing; the 180° meridian is highlighted and the limb of Jupiter is indicated (long-dashed line). The inset includes a scale bar that shows that the IFT emissions extend vertically over 1000 km above the limb of Jupiter. The inset is smoothed over 3 × 3 pixels; the brighter parts of the IFT footprint have a signal-to-noise ratio (SNR) of ~3.9, whereas the entire feature is detected at a SNR of ~33.